ISSN 1063-7788, Physics of Atomic Nuclei, 2016, Vol. 79, No. 3, pp. 326–334. © Pleiades Publishing, Ltd., 2016.
Original Russian Text © A.S. Danagulyan, G.H. Hovhannisyan, T.M. Bakhshiyan, G.V. Martirosyan, 2016, published in Yadernaya Fizika, 2016, Vol. 79, No. 3, pp. 220–228.

NUCLEI
Theory

# Special Features of Isomeric Ratios in Nuclear Reactions Induced by Various Projectile Particles

**A. S. Danagulyan, G. H. Hovhannisyan*, T. M. Bakhshiyan, and G. V. Martirosyan**

*Yerevan State University, Alek Manukyan Str. 1, Yerevan 0025, Republic of Armenia*

Received August 27, 2015

**Abstract**—Calculations for $(p, n)$ and $(\alpha, p3n)$ reactions were performed with the aid of the TALYS-1.4 code. Reactions in which the mass numbers of target and product nuclei were identical were examined in the range of $A = 44$–$124$. Excitation functions were obtained for product nuclei in ground and isomeric states, and isomeric ratios were calculated. The calculated data reflect well the dependence of the isomeric ratios on the projectile type. A comparison of the calculated and experimental data reveals, that, for some nuclei in a high-spin state, the calculated data fall greatly short of their experimental counterparts. These discrepancies may be due to the presence of high-spin yrast states and rotational bands in these nuclei. Calculations involving various level-density models included in the TALYS-1.4 code with allowance for the enhancement of collective effects do not remove the discrepancies in the majority of cases.

**DOI:** 10.1134/S1063778816020058

## INTRODUCTION

Experiments cannot be reasonably performed without thoroughly planning them or performing preliminary theoretical calculations. Existing models make it possible to plan experiments in various energy regions. In turn, new experimental data serve as a basis for continuously refining model concepts.

The TALYS code [1] permits calculations for reactions involving neutrons, protons, deuterons, tritons, alpha particles and gamma rays and proceeding at energies in the region extending up to 1 GeV (in the case of employing the TALYS-1.6 version). It also enables one to calculate total and partial reaction cross sections, energy spectra, and angular distributions, as well as double-differential spectra of reaction products. The package in question relies on the optical model and an extensive database of nuclear states. TALYS is permanently upgraded in accordance with current requirements. For example, a novel feature of the TALYS-1.4 code in relation to TALYS-1.2 is that the former includes a phenomenological model for nuclear decays, and this makes it possible to remove some problems in predicting cross sections. Also, the possibilities for the choice of form for the distributions of the nuclear-level density, which are necessary for calculations on the basis of the statistical model [2], became wider. Further, TALYS-1.6 presents extended options of output data, and it is possible now to obtain, in the output file, the reaction-product activity in MBq or Ci units as a function of time, and this is very convenient for planning experiments that involve the production of radionuclides [3].

There are many studies in which the authors state that calculations performed with the aid of the TALYS code lead to results that agree well with experimental data [4–8]. Our calculations for $(p, n)$, $(\alpha, p3n)$, $(^3\mathrm{He}, xn)$, and $(\alpha, xn)$ reactions and a comparison of their results with experimental data borrowed from the EXFOR database [9] made it possible to reveal cases in which there is a substantial discrepancy between theoretical predictions and experimental data.

## RESULTS AND DISCUSSION

In the present study, we examine isomeric ratios for nuclei produced in $(p, n)$ and $(\alpha, p3n)$ reactions, defining an isomeric ratio (IR) as the ratio of the production cross sections for a nucleus in a high-spin state and a state of lower spin, $R = \sigma_h/\sigma_l$. We choose reactions in which the mass numbers of target and product nuclei are identical, which makes it possible to analyze the dependence of IR values on the projectile type.

Isomeric ratios were calculated with the aid of the TALYS-1.4 code. The IR values obtained for 46 product nuclei are given in the table. The table also presents values of the ratio $R_{(\alpha,p3n)}/R_{(p,n)}$ and properties (spin, parity, and half-life) of target and product nuclei. The values of $R_{(d,2n)}/R_{(p,n)}$ for the same target nuclei can be found in [4]. The isomeric ratios in question were calculated at the maxima of

*E-mail: hov_gohar@ysu.am

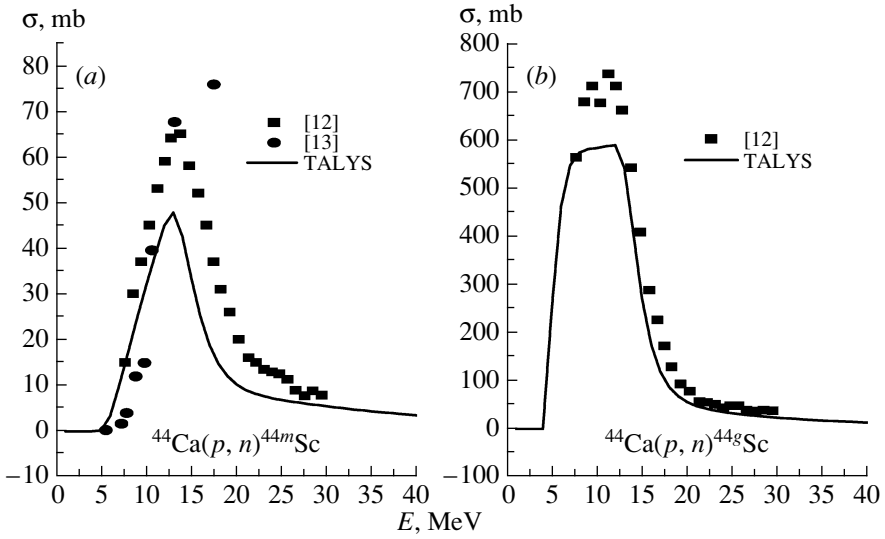


**Fig. 1.** Excitation functions for the reactions $^{44}\mathrm{Ca}(p,n)^{44m,g}\mathrm{Sc}$ according to experimental measurements and according to calculations based on the TALYS-1.4 code.

respective excitation functions. The table shows that the values of $R_{(\alpha,p3n)}/R_{(p,n)}$ range between 1.03 and 101.7, depending on the spin of the isomeric state. It is noteworthy that, in the case of high-spin isomers ($8^{\pm}$), the ratios $R_{(\alpha,p3n)}/R_{(p,n)}$ have the largest values (between 59 and 101). For lower spins ($7^{\pm}$ or $6^{\pm}$), the IR values are smaller.

A comparison of the cross sections calculated for $(p,n)$, $(\alpha,p3n)$, $(^3\mathrm{He},xn)$, and $(\alpha,xn)$ reactions with experimental data revealed that, in some cases, the discrepancies are quite sizable. In particular, the cross sections calculated for $^{44}_{21}$Sc, $^{86}_{39}$Y, and $^{87}_{39}$Y nuclei produced in a high-spin state are substantially smaller than their experimental counterparts; at the same time, agreement for the ground state is satisfactory. Thus, it becomes necessary to discuss nuclear reactions leading to the formation of these products.

Let us consider the $^{44}$Sc nucleus. The odd–odd nucleus of $^{44}$Sc is nearly magic in the number of protons ($Z = 21$), but it is deformed in the number of neutrons ($N = 23$)—that is, it has a nonzero intrinsic electric quadrupole moment. According to the shell model, the $1f_{7/2}$ subshell is filled in this nucleus.

In some nuclear reactions induced by various projectiles (deuterons, alpha particles, and ions), the nucleus involved remains cold despite the presence of a high excitation energy ($E^*$), since the whole energy goes to the formation of the angular momentum of the system [10]. Owing to a rotational collective motion, there arise high-spin yrast states.

An excited yrast level of spin–parity $15^-$ arises at $E = 9141$ keV in the case of the $^{44}$Sc nucleus [11]. After a sequence of electric dipole and quadrupole transitions, the nucleus goes over to the $10^+$ and $11^+$ states, whereupon the filling of the $6^+$ state occurs via collective transitions. The ground state, whose spin–parity is $2^+$, is also filled via yrast-line decay, albeit with a low probability [11].

The excitation functions for the isomeric and ground states in the reactions $^{44}\mathrm{Ca}(p,n)^{44m,g}\mathrm{Sc}$ are shown in Fig. 1 according to experimental data from [12, 13] and according to the results of the calculations based on the TALYS-1.4 code. The discrepancy between these experimental and theoretical results is about 46% for the isomeric state (see Fig. 1*a*) and about 17% for the ground state (see Fig. 1*b*).

The isomeric ratio as a function of the projectile energy in the reaction $^{44}\mathrm{Ca}(\alpha,p3n)^{44}\mathrm{Sc}$ is given in Fig. 2 according to experimental data from [12, 14] and according to theoretical calculations performed with the aid of the TALYS-1.4 code. In the energy region extending from 45 MeV upward, experimental data exceed substantially their calculated counterparts. In either case, the discrepancy is likely to be due to the filling of both states of the $^{44}$Sc product nucleus via the deexcitation of yrast states.

Within statistical models, a nuclear-level density function is used to calculate reaction cross sections in the cases where information about discrete excited levels of the nucleus involved is absent or is incomplete. The TALYS-1.4 code code includes various models for determining nuclear levels [2]. Three of them are phenomenological models that yield somewhat different distributions of the nuclear-level

Isomeric ratios ($R$), ratios $R_{(\alpha,p3n)}/R_{(p,n)}$, and spin–parities and half-lives for target and product nuclei

| Target | $I^p$ | Product nucleus | $m$-state of product nucleus | | $g$-state of product nucleus | | $R$ | | $R_{(\alpha,p3n)}/R_{(p,n)}$ |
|---|---|---|---|---|---|---|---|---|---|
| | | | $I^p$ | $T_{1/2}$ | $I^p$ | $T_{1/2}$ | $(p,n)$ | $(a,p3n)$ | |
| $^{86}$Sr | $0^+$ | $^{86}$Y | $8^+$ | 48 min | $4^-$ | 14.74 h | 0.054 | 3.42 | 63.3 |
| $^{116}$Sn | $0^+$ | $^{116}$Sb | $8^-$ | 60.3 min | $3^+$ | 15.8 min | 0.13 | 7.7 | 59.23 |
| $^{118}$Sn | $0^+$ | $^{118}$Sb | $8^-$ | 5.00 h | $1^+$ | 3.6 min | 0.081 | 5.76 | 71.1 |
| $^{120}$Sn | $0^+$ | $^{120}$Sb | $8^-$ | 5.76 d | $1^+$ | 15.89 min | 0.11 | 7.1 | 64.5 |
| $^{122}$Sn | $0^+$ | $^{122}$Sb | $8^-$ | 4.21 min | $2^-$ | 2.7 d | 0.06 | 6.1 | 101.7 |
| $^{124}$Sn | $0^+$ | $^{124}$Sb | $8^-$ | 20.2 min | $3^-$ | 60.2 d | 0.12 | 10.2 | 85 |
| $^{92}$Zr | $0^+$ | $^{92}$Nb | $7^+$ | $3.47 \times 10^7$ yr | $2^+$ | 10.15 d | 0.24 | 12.95 | 53.96 |
| $^{94}$Mo | $0^+$ | $^{94}$Tc | $7^+$ | 293 min | $2^+$ | 52 min | 2 | 53.1 | 26.6 |
| $^{96}$Mo | $0^+$ | $^{96}$Tc | $7^+$ | 4.28 d | $4^+$ | 51.5 min | 1.35 | 20.44 | 15.14 |
| $^{108}$Cd | $0^+$ | $^{108}$In | $7^+$ | 58 min | $2^+$ | 39.6 min | 0.23 | 1.31 | 5.7 |
| $^{11}$Cd | $0^+$ | $^{110}$In | $7^+$ | 4.9 h | $2^+$ | 69.1 min | 0.12 | 0.63 | 5.25 |
| $^{44}$Ca | $0^+$ | $^{44}$Sc | $6^+$ | 58.6 h | $2^+$ | 3.927 h | 0.09 | 1.69 | 18.8 |
| $^{52}$Cr | $0^+$ | $^{52}$Mn | $6^+$ | 5.591 d | $2^+$ | 21.1 min | 0.36 | 6.1 | 16.94 |
| $^{84}$Kr | $0^+$ | $^{84}$Rb | $6^-$ | 20.26 min | $2^-$ | 32.77 d | 0.15 | 0.36 | 2.4 |
| $^{86}$Kr | $0^+$ | $^{86}$Rb | $6^-$ | 1.017 min | $2^-$ | 18.63 d | 0.25 | 6.9 | 27.6 |
| $^{94}$Zr | $0^+$ | $^{94}$Nb | $6^+$ | $2.03 \times 10^4$ yr | $3^+$ | 6.263 min | 0.13 | 7.96 | 61.23 |
| $^{102}$Ru | $0^+$ | $^{102}$Rh | $6^+$ | 2.9 yr | $2^-$ | 207 d | 0.2 | 0.59 | 2.95 |
| $^{106}$Pd | $0^+$ | $^{106}$Ag | $6^+$ | 8.28 d | $1^+$ | 23.96 min | 0.34 | 21.72 | 63.9 |
| $^{108}$Pd | $0^+$ | $^{108}$Ag | $6^+$ | 418 yr | $1^+$ | 2.37 min | 0.22 | 0.6 | 2.73 |
| $^{110}$Pd | $0^+$ | $^{110}$Ag | $6^+$ | 249.8 d | $1^+$ | 24.6 s | 0.16 | 8.4 | 52.5 |
| $^{58}$Fe | $0^+$ | $^{58}$Co | $5^+$ | 9.15 h | $2^+$ | 70.82 d | 0.34 | 2.77 | 8.15 |
| $^{80}$Se | $0^+$ | $^{80}$Br | $5^-$ | 4.42 h | $1^+$ | 17.68 min | 0.49 | 1.05 | 2.14 |
| $^{82}$Se | $0^+$ | $^{82}$Br | $5^-$ | 35.3 h | $2^-$ | 6.13 min | 0.299 | 13.65 | 45.65 |
| $^{82}$Kr | $0^+$ | $^{82}$Rb | $5^-$ | 6.48 h | $1^+$ | 1.27 min | 0.69 | 19.68 | 28.5 |
| $^{100}$Ru | $0^+$ | $^{100}$Rh | $5^+$ | 4.6 min | $1^-$ | 20.8 h | 0.37 | 0.38 | 1.03 |
| $^{104}$Ru | $0^+$ | $^{104}$Rh | $5^+$ | 4.34 min | $1^+$ | 42.3 s | 0.37 | 15.1 | 40.8 |
| $^{102}$Pd | $0^+$ | $^{102}$Ag | $5^+$ | 12.9 min | $2^+$ | 7.7 min | 1.3 | 4.51 | 3.47 |
| $^{104}$Pd | $0^+$ | $^{104}$Ag | $5^+$ | 69.2 min | $2^+$ | 33.5 min | 0.57 | 26.03 | 45.7 |
| $^{114}$Cd | $0^+$ | $^{114}$In | $5^+$ | 49.51 d | $1^+$ | 71.9 s | 0.82 | 4.95 | 6.04 |
| $^{116}$Cd | $0^+$ | $^{116}$In | $5^+$ | 54.41 min | $1^+$ | 14.10 s | 0.81 | 3.65 | 4.5 |
| $^{112}$Cd | $0^+$ | $^{112}$In | $4^+$ | 20.56 min | $1^+$ | 14.97 min | 0.94 | 3.1 | 3.3 |
| $^{121}$Sb | $5/2^+$ | $^{121}$Te | $11/2^-$ | 154 d | $1/2^+$ | 16.78 d | 1.32 | 18.18 | 13.8 |
| $^{123}$Sb | $7/2^+$ | $^{123}$Te | $11/2^-$ | 119.7 d | $1/2^+$ | $1 \times 10^{13}$ yr | 1.66 | 1.01 | 0.61 |
| $^{77}$Se | $1/2^-$ | $^{77}$Br | $9/2^+$ | 4.28 min | $3/2^-$ | 57.04 h | 0.55 | 14.03 | 25.5 |
| $^{85}$Rb | $5/2^-$ | $^{85}$Sr | $9/2^+$ | 64.84 d | $1/2^-$ | 67.63 s | 2.69 | 38.97 | 14.49 |
| $^{87}$Sr | $9/2^+$ | $^{87}$Y | $9/2^+$ | 13.37 h | $1/2^-$ | 79.8 h | 4.69 | 25.76 | 5.49 |
| $^{89}$Y | $1/2^-$ | $^{89}$Zr | $9/2^+$ | 78.41 h | $1/2^-$ | 4.18 min | 1.1 | 35.9 | 32.6 |
| $^{91}$Zr | $5/2^+$ | $^{91}$Nb | $9/2^+$ | 680 yr | $1/2^-$ | 60.86 d | 1.39 | 0.92 | 0.66 |
| $^{95}$Mo | $5/2^+$ | $^{95}$Tc | $9/2^+$ | 20.0 h | $1/2^-$ | 61 d | 2.68 | 43.9 | 16.4 |
| $^{97}$Mo | $5/2^+$ | $^{97}$Tc | $9/2^+$ | $2.6 \times 10^6$ yr | $1/2^-$ | 90.1 d | 3.95 | 49.9 | 12.6 |
| $^{99}$Ru | $5/2^+$ | $^{99}$Rh | $9/2^+$ | 4.7 h | $1/2^-$ | 16.1 d | 2.63 | 25.2 | 9.6 |
| $^{101}$Ru | $5/2^+$ | $^{101}$Rh | $9/2^+$ | 4.34 d | $1/2^-$ | 3.3 yr | 2 | 14.37 | 7.2 |
| $^{111}$Cd | $1/2^+$ | $^{111}$In | $9/2^+$ | 2.81 d | $1/2^-$ | 7.7 min | 1.91 | 46.1 | 24.1 |
| $^{127}$I | $5/2^+$ | $^{127}$Xe | $9/2^-$ | 69.2 s | $1/2^+$ | 36.4 d | 1.04 | 15.6 | 15 |
| $^{105}$Pd | $5/2^+$ | $^{105}$Ag | $7/2^+$ | 7.23 min | $1/2^-$ | 41.29 d | 3.92 | 42.6 | 10.9 |
| $^{113}$In | $9/2^+$ | $^{113}$Sn | $7/2^+$ | 21.4 min | $1/2^+$ | 115.09 d | 18.9 | 92.2 | 4.9 |

density. These are the constant-temperature model (CTM), back-shifted Fermi gas model (BFM), and the generalized superfluid model (GSM). None of these models takes explicitly into account collective effects, but one can introduce a collective-effect-enhancement factor in nuclear-level density functions. Two other models for nuclear levels rely on a microscopic approach and employ tabulated data from the RIPL-3 database [2].

We have performed calculations for the reactions $^{44}\mathrm{Ca}(p,n)^{44m,g}\mathrm{Sc}$, employing all possible nuclear-level models. In Figs. 3–10 given below, we present the results of our calculations performed with (TALYS) the default nuclear-level density function, (*1*) the collective-effect-enhancement factor introduced in the CTM nuclear-level density functions, (*2*) the collective-effect-enhancement factor introduced in the BFM nuclear-level density functions, (*3*) with the collective-effect-enhancement factor introduced in the GSM nuclear-level density functions, (*4*) with the aid of a microscopic model based on Hartree–Fock calculations, and (*5*) with the aid of the combined Skyrme–Hartree–Fock–Bogolyubov model (where one takes collective effects into account). The introduction of the collective-effect-enhancement factor changes the results of the calculations for the isomeric state. The best agreement with experimental data is provided by the *2* and *5* models. The respective changes for the ground state are insignificant (see Figs. 3*a* and 3*b*).

Let us now consider the $^{86}_{39}\mathrm{Y}_{47}$ and $^{87}_{39}\mathrm{Y}_{48}$ nuclei. In them, protons fill the $2p_{1/2}$ shell, while neutrons fill the $1g_{9/2}$ shell. In the case of a nucleus featuring 47 neutrons, more than half of the $g_{9/2}$ subshell is filled, so that this nucleus is deformed. As the number of neutrons approaches the magic number of 50, the shape of the nucleus becomes ever closer to a spherical shape.

According to the scheme of excited levels that is presented for the odd–odd nucleus of $^{86}$Y in [22], the nucleus in question has three yrast bands. In all three bands, there occur magnetic and electric dipole cascade transitions ($M1$ and $E1$, respectively), as well as electric quadrupole ($E2$) transitions, and these transitions lead to the population of the isomeric state at $E = 218$ keV whose spin–parity and half-life are $I^p = 8^+$ and $T_{1/2} = 48$ min, respectively. The ground state, whose respective features are $I^p = 4^-$ and $T_{1/2} = 14.74$ h, is not populated via the decay of yrast lines.

In Fig. 4, the excitation functions for (Fig. 4*b*) ground and (Fig. 4*a*) isomeric states of the isotope $^{86}$Y in the reactions $^{86}\mathrm{Sr}(p,n)^{86m,g}\mathrm{Y}$ are given according to experimental data from [12, 15] and according to the results of theoretical calculations performed with the aid of the TALYS-1.4 code. One can see that the values calculated for the isomeric state with the aid of the TALYS code are substantially smaller than their experimental counterparts. Agreement between the respective results for the ground state is good. The reason behind these discrepancies may be rooted in the inconsistency between excited nuclear levels and their model concepts. Because the deexcitation of nuclei having yrast states via gamma-ray emission, the high-spin isomeric state of the final nucleus is produced with a higher probability than that predicted by the model. The introduction of the collective-effect-enhancement factor changes somewhat the results of the calculations, but this does not lead to agreement with experimental data in the case of the isomeric state (see Fig. 4*a*).

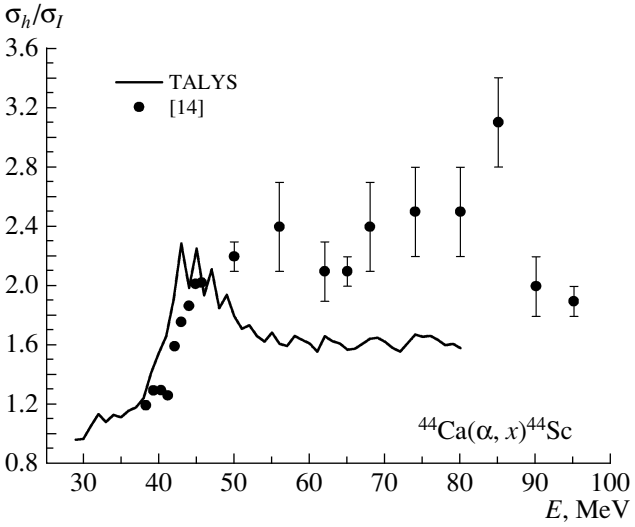


**Fig. 2.** Isomeric ratios versus the projectile energy in the reaction $^{44}\mathrm{Ca}(\alpha,p3n)^{44}\mathrm{Sc}$ according to experimental measurements and according to calculations based on the TALYS-1.4 code.

The excitation functions for the reactions $^{\mathrm{nat}}\mathrm{Rb}(^3\mathrm{He},\,xn)^{86m,g}\mathrm{Y}$ are given in Fig. 5. For the isomeric state, available experimental data [15, 16] exhibit a wide spread, but, in just the same way as in the case of the reaction $^{86}\mathrm{Sr}(p,n)^{86m}\mathrm{Y}$, the data calculated with the aid of the TALYS-1.4 code are well below their experimental counterparts. The calculations with the aid of the aforementioned models for nuclear-level densities do not lead to agreement with experimental data either (see Fig. 5).

Figure 6 shows the excitation functions for the reactions $^{85}\mathrm{Rb}(\alpha,xn)^{86m,g}\mathrm{Y}$. One can see that, in

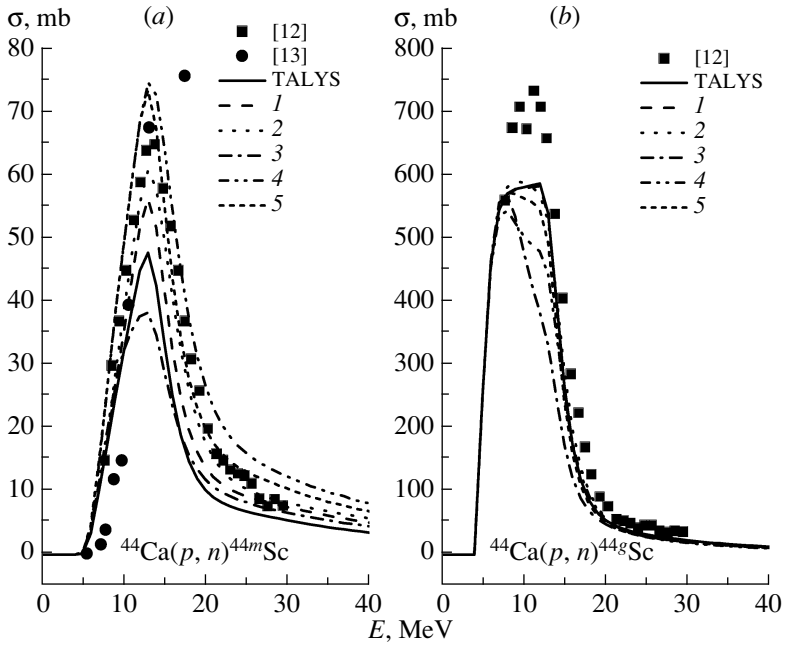


**Fig. 3.** Excitation functions for the reactions $^{44}Ca(p,n)^{44m,g}$Sc according to experimental data and results of calculations based on for all possible nuclear-level models (the notation used is explained in the main body of the text).

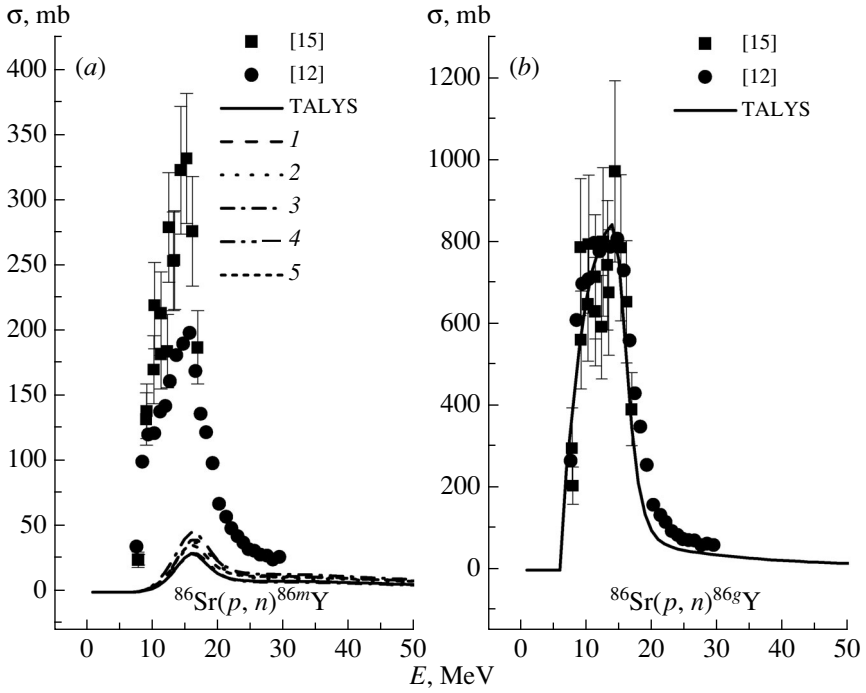


**Fig. 4.** As in Fig. 3, but for the reactions $^{86}$Sr$(p,n)^{86m,g}$Y.

either case, their experimental values from [12, 17] are in excess of the respective theoretical results.

The $^{87}$Y nucleus also has an yrast state of spin-parity $25/2^+$ at the energy of 3094.4 keV [23]. After several collective transitions, the $I^p = 9/2^+$ isomeric state of half-life $T_{1/2} = 13.37$ h at $E = 380.79$ keV, is populated, whereupon the ground state, whose spin–parity and half-life are $I^p = 1/2^-$ and $T_{1/2} =$

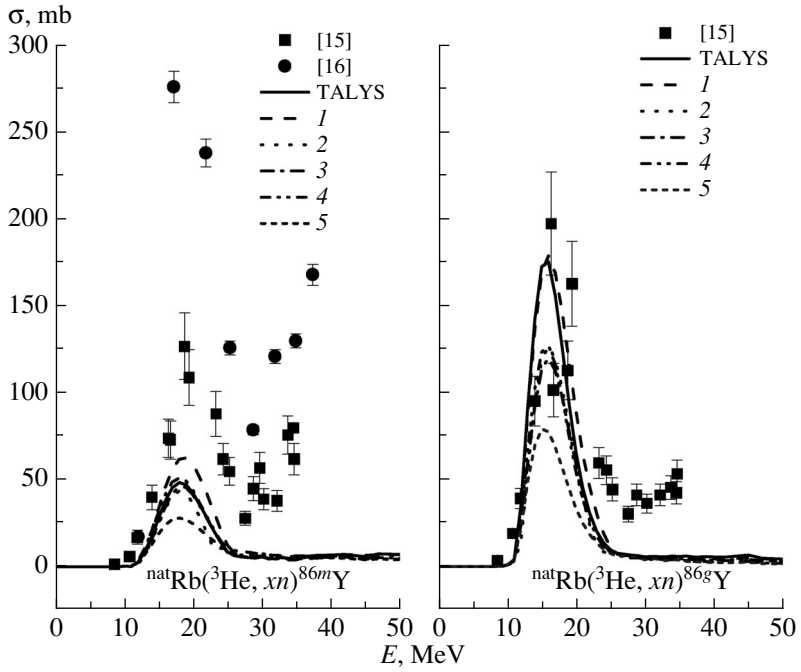


**Fig. 5.** As in Fig. 3, but for the reactions $^{\text{nat}}\text{Rb}(^3\text{He}, xn)^{86m,g}\text{Y}$.

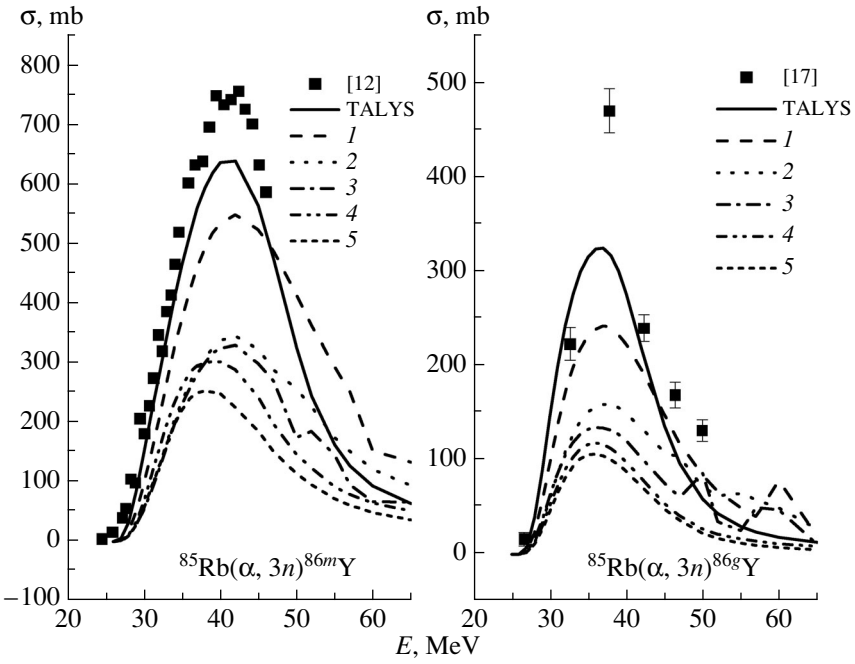


**Fig. 6.** As in Fig. 3, but for the reactions $^{85}\text{Rb}(\alpha, 3n)^{86m,g}\text{Y}$.

79.8 h, respectively, is filled via and $M4$ transition. Figure 7 gives the excitation functions for the reactions $^{87}\text{Sr}(p, n)^{87m,g}\text{Y}$. In that case, discrepancies between the calculated values and experimental results from [12] are observed both for the isomeric (see Fig. 7*a*) and for the ground state (see Fig. 7*b*).

The excitation functions for the reactions $^{\text{nat}}\text{Rb}(^3\text{He}, xn)^{87}\text{Y}$ and $^{85}\text{Rb}(\alpha, 2n)^{87}\text{Y}$ (see Figs. 8 and 9, respectively) demonstrate that, both for the

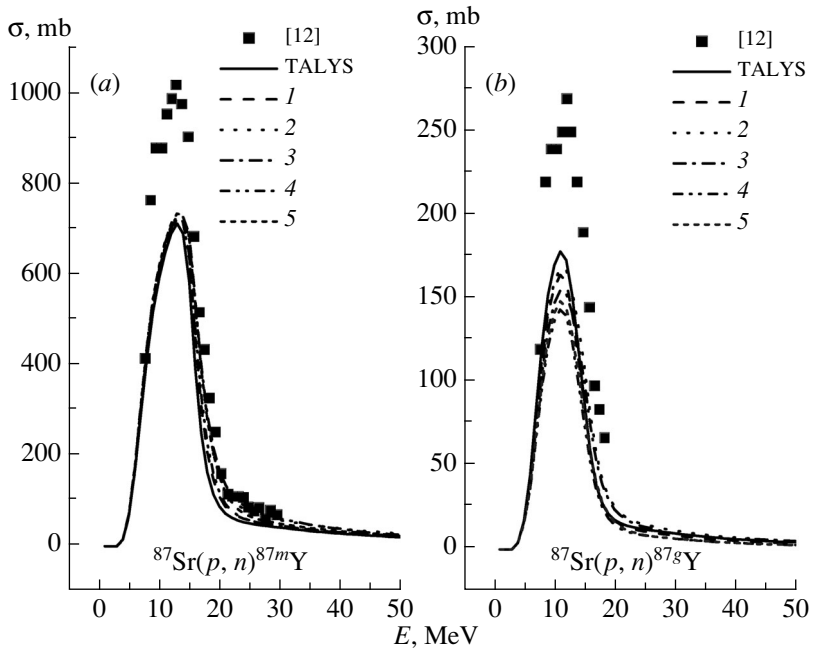


**Fig. 7.** As in Fig. 3, but for the reactions $^{87}\mathrm{Sr}(p,n)^{87m,g}\mathrm{Y}$.

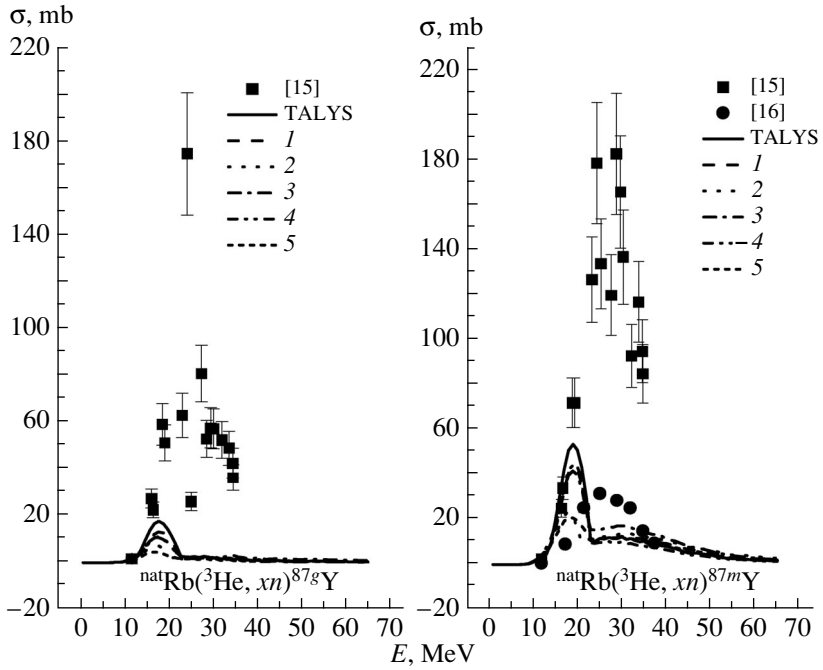


**Fig. 8.** As in Fig. 3, but for the reactions $^{\mathrm{nat}}\mathrm{Rb}(^3\mathrm{He},\, xn)^{87m,g}\mathrm{Y}$.

ground and for the isomeric states produced in these reactions, there are discrepancies between experimental data from [15, 16] and their theoretical counterparts calculated on the basis of the TALYS-1.4 code.

There are discrepancies between the measured and calculated data for the reaction $^{124}\mathrm{Sn}(p,n)^{124}\mathrm{Sb}$ as well (see Fig. 10). In the case of the $^{124}$Sb nucleus, we have found experimental data only for the ground

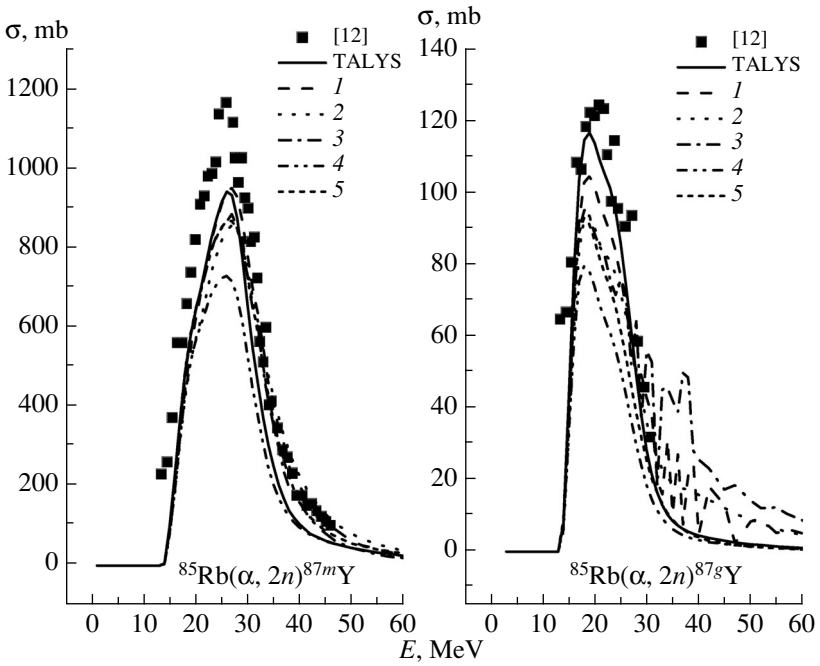


**Fig. 9.** As in Fig. 3, but for the reactions $^{85}\mathrm{Rb}(\alpha, 2n)^{87m,g}\mathrm{Y}$.

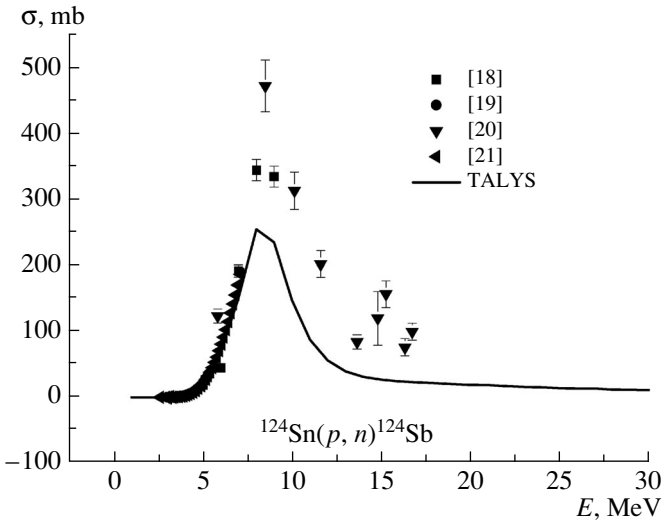


**Fig. 10.** As in Fig. 1, but for the reaction $^{124}\mathrm{Sn}(p, n)^{124}\mathrm{Sb}$.

state, whose spin–parity is $3^-$. The antimony nucleus possesses yrast states [24], whose decay leads to an increase in the probability for the formation of its high-spin states. The decay of the isomeric state $8^-$ contributes 75% to the population of the ground state. Therefore, the discrepancy in question may be due to the fact that this product nucleus has yrast lines.

## CONCLUSIONS

The calculations performed in the present study with the aid of the TALYS-1.4 code and aimed at determining cross sections for proton-induced and alpha-particle-induced nuclear reactions that lead to the formation of the ground and isomeric states of product nuclei have revealed that the respective model-based data reflect well the projectile-type dependence of isomeric ratios. We have considered reactions in which the mass numbers of target and product nuclei are identical.

We have noticed that, in some cases, experimental data differ strongly from their calculated counterparts. We have observed disagreements

primarily for high-spin states. We have examined the reactions $^{44}$Ca$(p,n)^{44}$Sc, $^{44}$Ca$(\alpha,p3n)^{44}$Sc, $^{86}$Sr$(p,n)^{86}$Y, $^{87}$Sr$(p,n)^{87}$Y, $^{\text{nat}}$Rb($^{3}$He, $xn)^{86,87}$Y, $^{85}$Rb$(\alpha,xn)^{86,87}$Y, and $^{124}$Sn$(p,n)^{124}$Sb. The discrepancies in question may be due to the presence in product nuclei of high-spin yrast states and rotational bands, whose deexcitation through electric dipole and quadrupole and magnetic dipole gamma transitions populates high-spin states. One observes yrast states ion-nucleus reactions [11, 22, 23]. However, we believe that the discrepancies between the model and experimental data in $(p,n)$ reactions is also due to the presence of yrast states in the nuclear products being considered.

## REFERENCES


1. http://www.talys.eu/
2. A. J. Koning, S. Hilaire, and S. Goriely, *TALYS-1.4 User Manual* (NRG, The Netherlands, 2011).
3. A. J. Koning, S. Hilaire, and S. Goriely, *TALYS-1.6 User Manual* (NRG, The Netherlands, 2013).
4. T. M. Bakhshiyan, Phys. Atom. Nucl. **79**, 38 (2016).
5. V. M. Mazur, Z. M. Bigan, D. M. Symochko, and T. V. Poltorzhytska, Phys. Part. Nucl. Lett. **179**, 248 (2012).
6. Mayeen Uddin Khandaker, Kwangsoo Kim, Kyung Sook Kim, et al., J. Korean Phys. Soc. **53**, 1181 (2008).
7. I. L. Rakhno, N. V. Mokhov, and K. K. Gudima, Fermilab-Conf-14-173-APC.
8. F. Tarkanyi, F. Ditroi, A. Hermanne, et al., Nucl. Instrum. Methods Phys. Res. B **269**, 1389 (2011).
9. https://www-nds.iaea.org/exfor/exfor.htm
10. A. Bohr and B. Mottelson, *Nuclear Structure,* vol. 2: *Nuclear Deformations* (Benjamin, New York, 1975), p. 50; J. R. Grover, Phys. Rev. **157**, 832 (1967).
11. M. Lach, J. Styczeń, W. Meczyński, et al., Eur. Phys. J. A **25**, 1 (2005).
12. V. N. Levkovskii, *Cross Sections for the Activation of Medium-Mass (A = 40–100) Nuclides by Intermediate-Energy (E = 10–50 MeV) Protons and Alpha Particles* (Inter-Vesy, Moscow, 1991) [in Russian].
13. S. Krajewski, I. Cydzik, K. Abbas, et al., Radiochim. Acta **101**, 333 (2013).
14. E. A. Bogila, V. I. Gavrilyuk, V. A. Zheltonozhskii, et al., Bull. Acad. Sci. USSR, Phys. Sec. **55** (5), 48 (1991).
15. F. Rösch, S. M. Qaim, and G. Stöcklin, Radiochim. Acta **61**, 1 (1993).
16. Y. Homma, M. Ishii, and Y. Murase, Appl. Radiat. Isot. **31**, 399 (1980).
17. A. Agarwal, M. K. Bhardwaj, I. A. Rizvi, and A. K. Chaubey, Indian J. Pure Appl. Phys. **41**, 829 (2003).
18. V. G. Batij and E. A. Skakun, in *Proceedings of the 41th Conference on Nuclear Spectroscopy and Nuclear Structure, Minsk, 1991,* p. 248.
19. C. H. Johnson and R. L. Kernell, Phys. Rev. C **2**, 639 (1970).
20. E. K. Elmaghraby, S. A. Said, and F. I. Asfour, Appl. Radiat. Isot. **67**, 147 (2009).
21. C. H. Johnson, J. K. Bair, C. M. Jones, et al., Phys. Rev. C **15**, 196 (1977).
22. Jian Li, C. Y. He, Y. Zheng, et al., Phys. Rev. C **88**, 014317 (2013).
23. E. K. Warburton, J. W. Olness, S. J. Lister, et al., J. Phys. G **12**, 1017 (1986).
24. T. Fenyes et al., Acta Phys. Hung. **71**, 239 (1992).